Dalton Transactions

PAPER

View Article Online
View Journal | View Issue

Cite this: *Dalton Trans.*, 2019, **48**, 6273

Direct intramolecular carbon(sp^2)–nitrogen(sp^2) reductive elimination from gold(III)†

Jong Hyun Kim,[a] R. Tyler Mertens,[a] Amal Agarwal,[a] Sean Parkin,[a] Gilles Berger[b] and Samuel G. Awuah*[a]

Received 30th December 2018,
Accepted 21st March 2019

DOI: 10.1039/c8dt05155k

rsc.li/dalton

The reactivity of bidentate Au^{III}–Cl species, [(C^N)$AuCl_2$], with a bisphosphine or carbon donor ligands results in reductive elimination. Combined experimental and computational investigations lead to the first evidence of a direct intramolecular C(sp^2)–N(sp^2) bond formation from a monomeric [(C^N)$AuCl_2$] gold (III) complex. We show that bidentate ligated Au(III) systems bypass transmetallation to form C(sp^2)–N(sp^2) species and NHC–Au–Cl. Mechanistic investigations of the reported transformation reveal a ligand-induced reductive elimination *via* a key Au^{III} intermediate. Kinetic studies of the reaction support a second-order rate process.

Introduction

Rudimentary steps associated with transition metal-catalyzed processes can be appropriately tuned to improve reaction efficiency.[1,2] Additionally, synthesis of stable metal complexes in the process requires innovative synthetic maneuvering. Reductive elimination affords a key product-releasing step in catalytic and stoichiometric transformations in organic synthesis. The use of d^8 metal centers including palladium(II), platinum(II), and nickel(II) to form new C–C and C–X (X = S, O, I, N, P) bonds has been well studied and its mechanistic insights sufficiently unraveled.[3–6] These studies have led to useful cross-coupling reactions, such as the formation of arylamines from C(sp^2)–N elimination, evidenced by the Buchwald–Hartwig cross-coupling reaction.[7,8] Other high-valent Pt^{IV}, Pd^{IV}, Ni^{IV} and Rh^{III} complexes have been employed in reductive C–X bond formation.[9–14] While these have been well advanced, synthetic transformations associated with Au(III) need further exploration. Thus, a vast chemical space exists to explore reductive elimination using gold centers.[15–17]

Reductive elimination can be an intricate part of decomposition mechanisms associated with transition metal compounds with high oxidation states including gold(III).[18,19] In seminal investigations, Kochi[20–22] and Tobias[23] showed carbon–carbon coupling using alkylgold(III) and Vicente demonstrated that unsymmetrical biaryls can be generated *via* carbon–carbon coupling from *cis*-diarylgold(III) with the concomitant Au(I) species formed as proof of reductive elimination[24,25] (Scheme 1A). The work by Toste probed the kinetic rates of carbon–carbon reductive elimination[26] *via* associative ligand exchange (Scheme 1B) and further investigated halide-dependent mechanisms of reductive elimination of Au(III).[5,27]

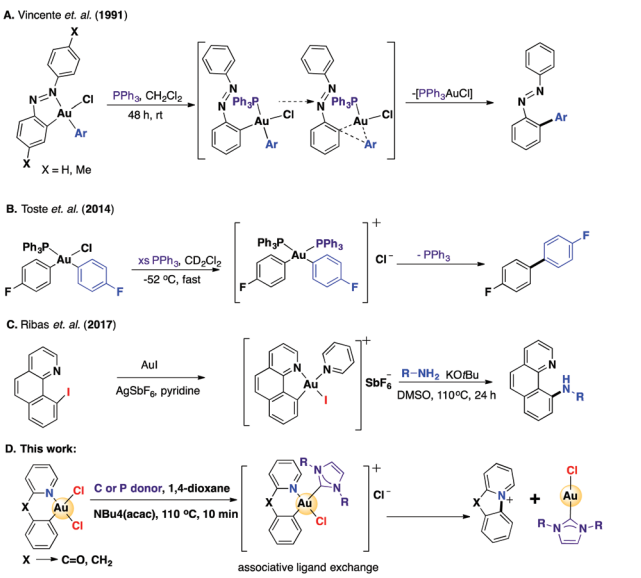

Scheme 1 Ligand-induced reductive elimination involving Au^{III} halide species. (A–B) C–C reductive elimination from gold. (C) Precedent for a gold(I)-catalyzed intermolecular C–N bond. (D) Evidence for intramolecular C–N bond formation from gold(III).

[a]*Department of Chemistry, University of Kentucky, 505 Rose Street, Lexington, Kentucky 40506, USA. E-mail: awuah@uky.edu*
[b]*Microbiology, Bioorganic & Macromolecular Chemistry, Faculty of Pharmacy, Université Libre de Bruxelles, Belgium*

†Electronic supplementary information (ESI) available: Materials and methods, synthesis and characterization of compounds, coordinates for DFT-computed structures, crystallographic data for compound **3**, spectral data and kinetic plots. CCDC 1845793 (**3**) and 1869535 (**IM2**). For ESI and crystallographic data in CIF or other electronic format see DOI: 10.1039/c8dt05155k

Recent examples of $C(sp^2)$–$C(sp^2)$,[28–31] $C(sp^2)$–X,[32,33] and $C(sp^2)$–N[34–36] (Scheme 1C) bond formation from putative monomeric species of Au(III) reveal electronic and steric impact on the reactivity and synthesis. Work so far to understand the fundamentals of Au-catalyzed $C(sp^2)$–N formation as well as electronic and steric effects on reaction rates and mechanisms remains unexplored.

We envisioned that reductive elimination from a rigid cyclic biaryl system facilitated with a nucleophile would be a representative model to study $C(sp^2)$–$N(sp^2)$ bond formation and importantly offer an operationally simple but rapid strategy to access Au(I) for potential applications (Scheme 1D). Specifically, phosphine coordinating ligands and *in situ*-generated carbene nucleophiles could induce intramolecular $C(sp^2)$–N formation from a well characterized cyclometalated (*C*,*N*) Au(III) motif. The example of the gold-mediated C–N reductive elimination presented leads to the concomitant generation of NHC–Au–Cl or NHC–Au–NHC under normal atmospheric conditions in low to moderate yields. Additionally, mechanistic insights into and kinetic investigations on this novel reaction system are described.

Results and discussion

Cognizant of the stability of (*C*,*N*)-cyclometalated Au(III) complexes, we designed a strategy that would employ the neutral, cyclometalated gold(III) motifs, **1** and **1′**. We found these complexes to be air-stable and, in addition, bearing carbon atoms that could yield a favorable five-membered cyclized product following reductive C–N bond formation.

The reactivity of the well-defined complex towards reductive elimination was next explored. Using an equimolar suspension of **1** or **1′** and imidazolium salts (**2a–e**) in 1,4-dioxane, the solution was heated at 100 °C in the presence of a tetrabutylammonium acetylacetonate salt (NBu_4(acac), Scheme 2). As expected, ^{1}H-NMR of the reaction mixture after 10 min showed complete disappearance of the methine peak of imidazolium salts (**2a–e**), indicative of carbene formation, which facilitates conversion to the respective reductively eliminated Au(I) products, **3** and **4a–e** from **1**. The reaction yields for **3** varied depending on the substrate, typically ranged from 7% to 73% as deduced by proton NMR. We reason that the X-ray structure of $[(C\hat{}N)AuCl_2]$[37] reveals a longer Au–Cl bond trans to the aryl carbon, which provides feasibility for ligand exchange with approaching donor ligands.

We were fortunate to obtain single crystals from slow evaporation of the reaction mixture. The yellow crystals were suitable for X-ray diffraction (Fig. 1). The structure of **3** shows a slightly puckered planar geometry with C–N bond distances comparable to those of other benzoylpyridinium salts.[38]

Given that most reductive elimination studies are driven by thermolysis, we conducted control experiments to demonstrate that the observed C–N bond formation was not simply a result of thermal elimination, but a nucleophile-promoted reductive elimination. Compound **4a** was not observed when **1** was heated to 100 °C in 1,4-dioxane or 80 °C in acetonitrile for 10 min. Furthermore, in support of nucleophile-promoted reductive elimination, treatment of **2a** with **1** without a base did not produce **3** or **4a** (Fig. S39†). We hypothesized that *in situ* carbene generation following the deprotonation of the methine proton in **2a** by NBu_4(acac), $NaHCO_3$, or KO*t*Bu results in a carbon nucleophile that initiates reductive elimination. We note that the use of NBu_4(acac) leads to a clean conversion to reductive elimination products in a remarkably shorter time of 10 min, compared to relatively longer reaction times with $NaHCO_3$ or KO*t*Bu. It can be attributed to the strong basicity of NBu_4(acac), which contributes to its effectiveness as a base in the presence of gold. We further expanded the scope of nucleophiles to study the effect of the electronic and steric diversity of imidazolium salts on reductive elimination (Scheme 2). Salts bearing aromatic substituents generated clean reactions with no side products. For assessing the functional group tolerance of this reaction, we used an imidazolium salt with a phenolic group (**2c**) as the carbene source. To our delight, NHC–Au(I)–Cl, **4c**, formed bearing phenolic side arms.

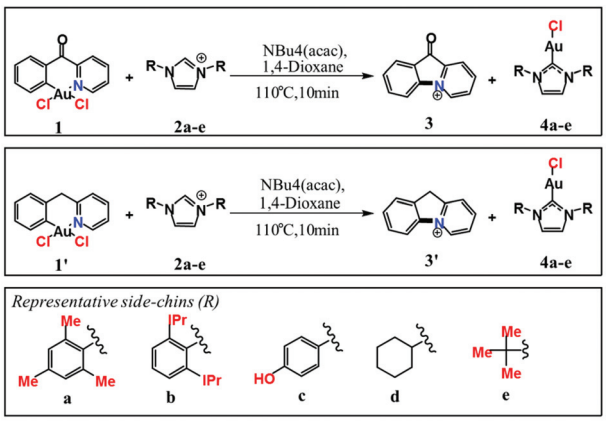

Compound	3 / 4a	3 / 4b	3 / 4c	3 / 4d	3 / 4e
Yield (%)	40 / 51	47 / 56	44 / 14	7 / 56	73 / 88
Compound	3′ / 4a	3′ / 4b	3′ / 4c	3′ / 4d	3′ / 4e
Yield (%)	56 / 51	48 / 37	73 / 42	40 / 39	64 / 60

Scheme 2 Carbene-promoted reductive elimination from organogold(III).

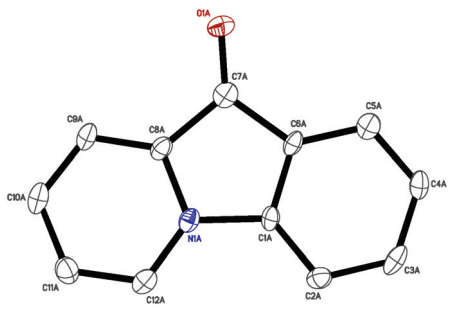

Fig. 1 X-ray crystal structure of **3**. Thermal ellipsoids set at 50% probability. For **3**, a single cation is shown; the actual structure had two crystallographically independent cations plus an extended polymeric $[AgCl_2]$ chain anion.

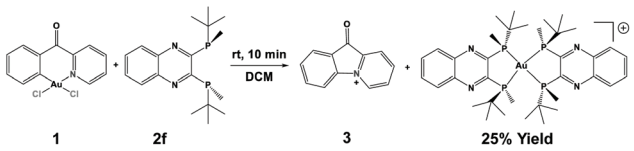

Scheme 3 Phosphine-promoted reductive elimination from organogold(III).

Having established the reactivity of the (*C*,*N*)-cyclometalated gold(III) complex, **1**, towards reductive elimination, we tested whether phosphine coordination could achieve the same result (Scheme 3). Bidentate phosphine, **2f**, showed rapid conversion (5 min) to a Au(I) phosphine complex and the pyridinium cation (**3**) at room temperature, and the product was confirmed by X-ray crystallography as in Fig. 1 and mass spectrometry. Overall, we discovered a reductive elimination protocol for an unprecedented C(**sp**^{2})–N(**sp**^{2}) bond formation using imidazolidene or phosphine ligands with NHC–Au(I)–Cl or phosphine–Au(I) compounds. From these studies, we demonstrated that C(**sp**^{2})–N bonded and Au(I) compounds can be generated rapidly from neutral Au(III) in respectable yields under air-stable conditions for numerous applications.

Kinetic studies for the steric and electronic properties of the NHC and [(C^N)AuCl$_2$]

Mechanistic underpinnings of the described reductive C–N bond formation were derived from ^{1}H-NMR spectroscopic studies. Mixtures of various molar equivalents of complex **1**, **2a**, and NBu$_4$(acac) in CD$_3$CN at 80 °C were used as model reactions. Consumption of **1** in acetonitrile followed second-order reaction kinetics, which were monitored by integrating peaks from **2a** or **4a** (Fig. 2(a) and S42–45†).

Kinetic investigations of the reaction of **1** with **2a** (using NBu$_4$(acac); equiv. = 0.75, 1.00, 1.25, 1.50 and 1.75) under second-order conditions were performed, inspired by the proposed mechanism of the reductive elimination process. Second-order dependence on the reactants was observed, as highlighted by the linear dependence of **1**/[**2a**] *versus* time when equimolar starting concentrations of **1** and **2a** were used (Fig. 2(b) [NBu$_4$(acac) ≈ activated **2a**]). In addition, a plot of the rate *versus* concentration in Fig. S50† shows a non-linear relationship, indicative of a second-order process. NMR monitoring of the conversion of **2a** enabled the determination of an experimental rate constant (k = 0.1080 to 1.9286 M^{-1} s^{-1} from 0.01024 to 0.01610 M). The reaction rate was accelerated by increasing the NBu$_4$(acac) concentration, indicative of a kinetic salt effect.

An Eyring analysis over a temperature range (24–80 °C) in CH$_3$CN provided kinetic parameters of the rate-determine step, $\Delta H^{\neq}$ = 6.4 ± 1.2 kcal mol^{-1}, $\Delta S^{\neq}$ = −0.044 ± 0.004 kcal mol^{-1} K, and $\Delta G^{\neq}$ = 18.3 ± 0.07 kcal mol^{-1} at 273.15 K (Fig. S51†). This reveals that the reductive elimination from Au(III) has not only a low enthalpy of activation but also a negative entropy of activation, which is consistent with the proposed associative mechanism.

We then chose **2e** as a substrate for comparative kinetic studies to evaluate the steric and electronic effects of NHCs on the overall reaction. The reaction was performed under similar experimental conditions (*i.e.* CD$_3$CN at 80 °C) to those described for **2a**. To monitor the reaction, the peaks were integrated from **2e** and **4e** (7.60 and 7.28 ppm, respectively), which were the protons on the imidazole ring (Fig. S46–48†). Similar to the reaction of **1** with **2a**, the reaction of **1** with **2e** follows a second order profile. Strikingly, Fig. 2(c) shows that the reaction of **1** with **2a** is 20 times faster than that of **1** with **2e**. Mesitylene groups of **2a** seem to make a positive contribution to the increased reaction rate, which is in good agreement with previous data that measured the nucleophilicity of NHCs.[39] In addition, we probed how the electron properties of [(C^N)AuCl$_2$] affected the rate by performing the reaction with **1′**, **2a**, and NBu$_4$(acac) (1.75 equiv.) in CD$_3$CN at 80 °C.

The proton peaks at 7.18 or 7.12 ppm of **2a** and **4a**, respectively, were used to monitor the reaction. A second order kinetic profile was deduced. In Fig. 2(d), a significant difference in reaction rates is observed; the reaction of **1** with **2a** was 14 times faster than that of **1′** with **2a**. The only distinction between **1** and **1′** is the carbonyl *vs.* methylene group, respectively. The carbonyl group is likely to impart electron withdrawing effects that make the gold center more electropositive relative to the methylene cyclometalated gold, **1′**. The improved reactivity of **1** as a result of the benzoylpyridine ligand dictates the rate of the reaction. In support of this phenomenon, we calculated Fukui indices using three different atomic charge schemes (Mulliken and Löwdin charges, as well as Hirshfeld partitioning), and the indices were calculated as previously described.[40] All three charge methods delivered an increased electrophilicity at the Au center for **1** in comparison with **1′** (see the ESI† for details). For reliable results, an all-electron relativistic approximation (zeroth order regular approximation, ZORA) was used together with ORCA 4.[41,42] Taken together, the experimental kinetics are consistent with ligand-induced reductive elimination, a clear departure from the zero- or first-order kinetics widely reported for unimolecular thermolysis.

Theoretical studies of the reaction mechanism

To gain insight into the mechanism of the reaction and its energy profile, we turned to DFT calculations. A first stable intermediate by associative ligand-exchange was calculated to be 13.8 kcal mol^{-1} lower in free energy than the approaching reactants (**IM1**, Fig. 3). We experimentally detected the intermediate, **IM1** *via* ESI-MS (Fig. S54†). A first transition state (**TS1**), 9.3 kcal mol^{-1} above the reactant complex, was found to precede the formation of **IM1**, as confirmed by intrinsic reaction coordinate calculations (IRC). An elongated Au–Cl bond at 2.68 Å, *trans* to the Au–C bond of the cyclometalated Au(III) complex, was observed with an approaching carbene, confirming the associative ligand-exchange proposition. Following the formation of the Au(III) intermediate **IM1**, we observed a second transition state (**TS$_{2a}$**), only 6.8 kcal mol^{-1} above the **IM1** level. Although two possible pathways to *C–N* reductive

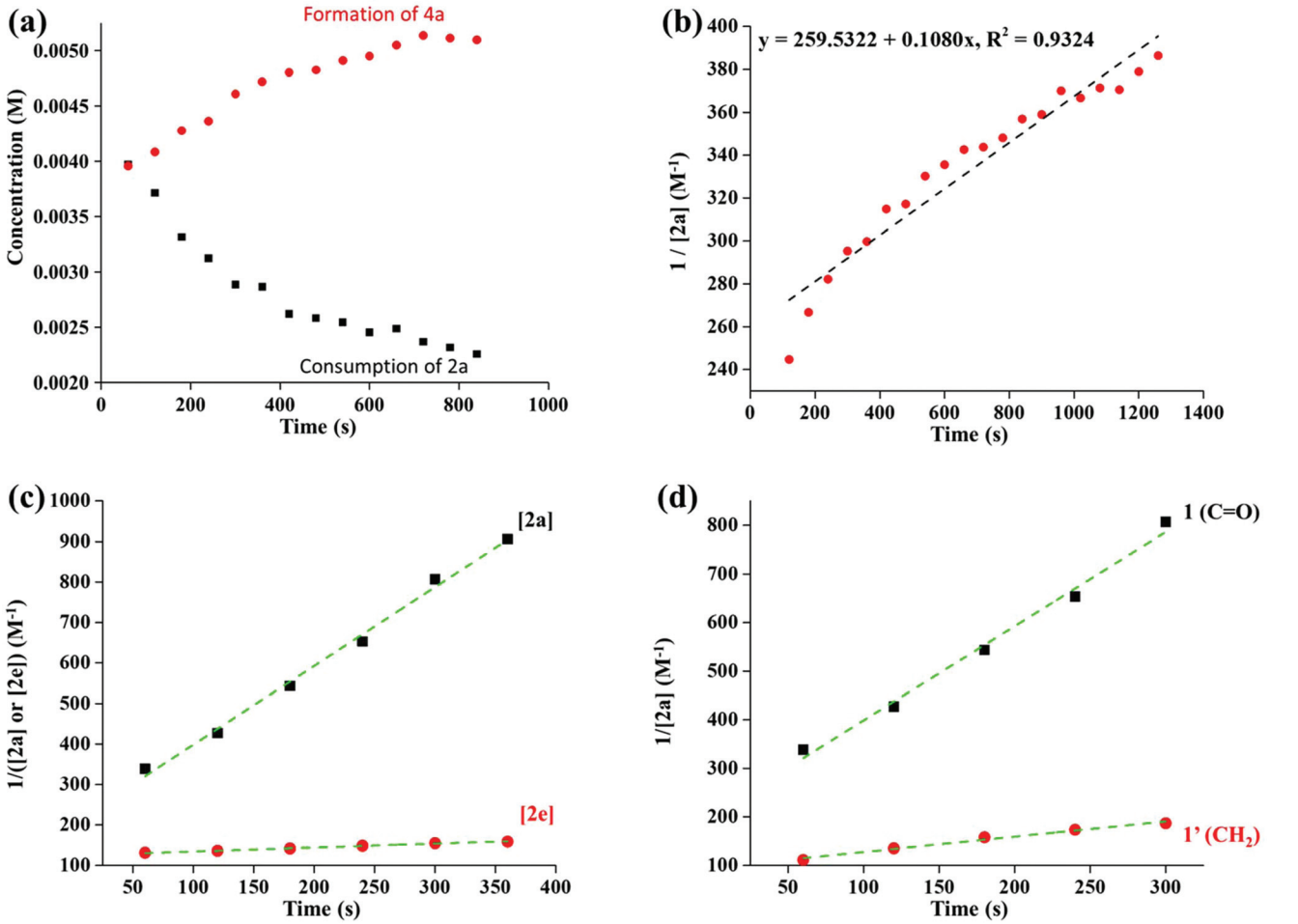

Fig. 2 (a) Reaction profile for the formation of **4a** from **1** monitored by ^{1}H-NMR and the consumption of **2a**. (b) A linear plot of **1**/[**2a**] *vs.* time implies second-order kinetics, k is 0.1080 M^{-1} s^{-1}, 1.00 equiv. of $NBu_4(acac)$ at 80 °C. (c) Comparison of reaction rates: ■ represents the reaction of **1** and **2a** and ● is for that of **1** and **2e**. Both experiments were performed at 80 °C and 1.75 equiv. of $NBu_4(acac)$ were used, respectively. k is 1.9286 M^{-1} s^{-1} (R^2 = 0.9966) for ■ and 0.0954 M^{-1} s^{-1} for ● (R^2 = 0.9944). (d) Comparison of reaction rates: ■ represents the reaction of **1** and **2a** and ● is for that of **1′** and **2a**. Both experiments were performed at 80 °C and 1.75 equiv. of $NBu_4(acac)$ were used, respectively. k is 1.9286 M^{-1} s^{-1} (R^2 = 0.9966) for ■ and 0.3111 M^{-1} s^{-1} for ● (R^2 = 0.9907).

elimination were envisaged, no theoretical evidence supports a concerted mechanism during which the Au–N bond is cleaved while the new C–N sp^2 is formed. Indeed, for the second pathway, two subsequent events were found, which first involve the breakage of the metal–nitrogen bond through a trigonal pyramidal transition state (**TS$_{2a}$**), well-known for substitutions on square pyramidal complexes (here, the attack of the chloride ion back on the metal center) and, secondly, the formation of the tricyclic aromatic system (**TS$_{2b}$**, $\Delta G^{\ddagger}$ = 4.0 kcal mol^{-1}), concomitantly with the release of the Au(I) complex and the chloride ion. This reductive elimination step further brings a strong thermodynamic drive to the reaction. This was also confirmed by IRC pathways (Fig. 3). Therefore, the experimentally elucidated X-ray structure of **3** coupled with ESI-MS of the key intermediate (**IM1**) in combination with computational methods lead to the proposed mechanism of intramolecular *C–N* reductive elimination *via* associative ligand exchange.

General information

All reagents were purchased from Oakwood Chemicals, VWR, Acros, or Aldrich, and used without further purification. Compounds **1** and **1′** were prepared according to literature procedures and well characterized prior to usage.[43,44] All reactions were carried out under normal atmospheric conditions. Deuterated solvents were purchased from Cambridge Isotope Laboratories (Andover, MA). ^{1}H NMR spectra were recorded on a Varian Unity 400/500 NMR spectrometer with a Spectro Spin superconducting magnet in the University of Kentucky NMR facility. Chemical shifts in ^{1}H NMR spectra were internally referenced to solvent signals (^{1}H NMR: DMSO at δ = 2.50 ppm and $CDCl_3$ at δ = 7.26). Electrospray ionization mass spectrometry (ESI-MS) was performed on an Agilent Technologies 1100 series liquid chromatography/MS instrument. High-resolution mass spectra (HRMS) were obtained by direct flow injection (injection volume = 5 or 2 μL) Electrospray Ionization

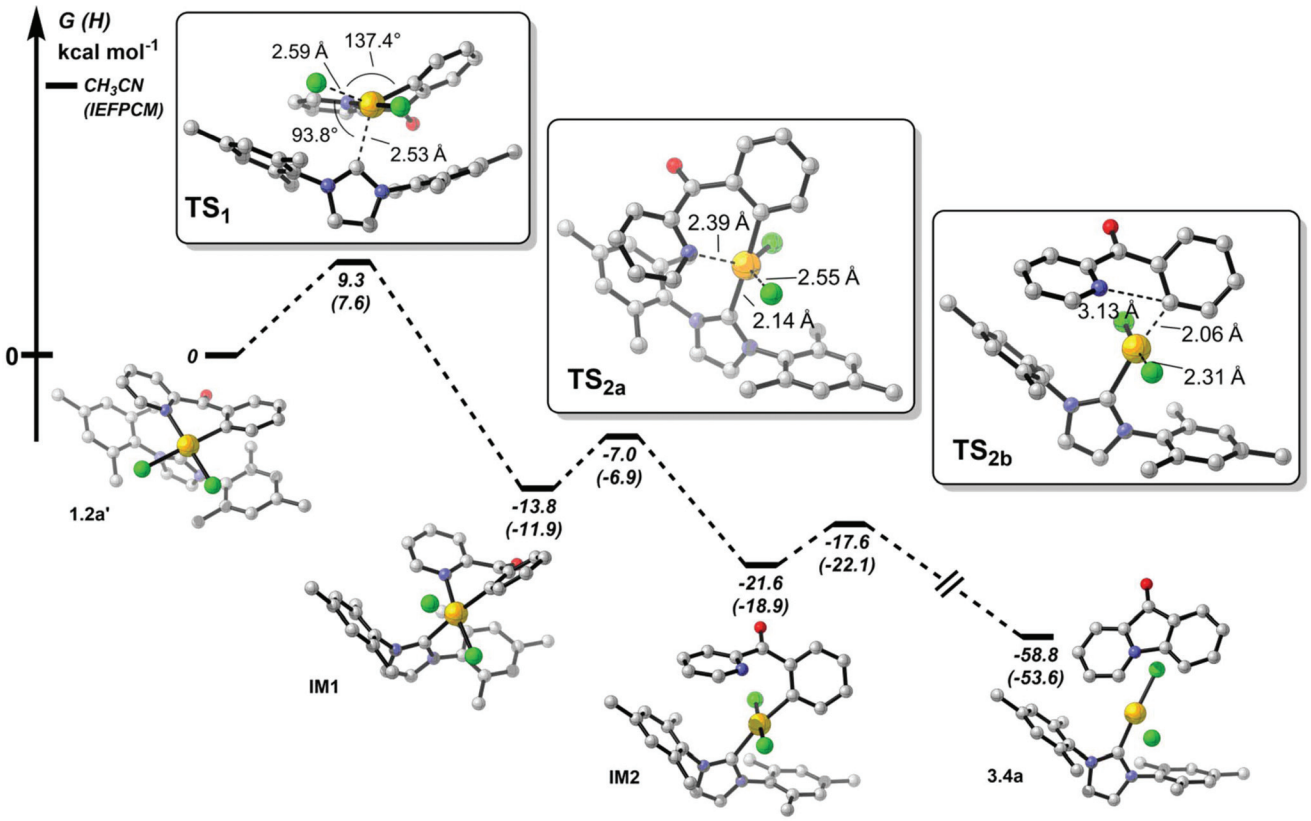

Fig. 3 Computed overall free energy profile of the intramolecular *C–N* reductive elimination process at the ωB97x-D/def2-TZVP level of theory in implicit acetonitrile.

(ESI) was performed on a Waters Qtof API US instrument in the positive mode (CIC, Boston University). Typical conditions are as follows: capillary = 3000 kV, cone = 35 or 15, source temperature = 120 °C, and desolvation temperature = 350 °C. The bulk purity of new compounds was assessed by combustion elemental analysis for C, H, and N. Elemental analysis was carried out at the microanalysis lab at the University of Illinois Urbana Champaign using PerkinElmer 2440, Series II with a combustion temperature of ~2000 °C and an accuracy of 0.3% abs. Reactions were monitored using aluminum backed silica-gel thin-layer chromatography (TLC) plates (Silicycle, TLA-R10011B-323, Canada) and visualized under low-wavelength light (254 nm) or stained with iodine on silica for visualization with the naked eye. Purification of reactions was performed using silica-gel (Silicycle, P/N: R10030B (SiliaFlash®F60, Size: 40–63 μm, Canada)) chromatography. A CombiFlash® Rf+Lumen, Teledyne ISCO, was used for purification of some compounds. Quantum chemical calculations using Gaussian[45] were performed in the University of Kentucky high-performance computing (HPC) facility.

Synthesis of Au(IMes)Cl (4a). Under normal atmospheric conditions, dichloro(2-benzoylpyridine)gold(III), **1** (20 mg, 0.04 mmol) and **2a** (15 mg, 0.04 mmol) were dissolved in 5 ml of 1,4-dioxane with NBu_4(acac) (29 mg, 0.09 mmol), and the solution was stirred and refluxed at 110 °C for 20 minutes. The color changed from pale yellow to purple and the reaction solution was monitored by TLC in 5% MeOH–DCM. **4a** showed a spot of $R_f \sim 0.9$ and $R_f \sim 0.8$ is for **3** on TLC. **4a** was separated by silica-gel chromatography with DCM as the eluent (yield: 12 mg, 51%) and then the eluent was changed to 25% ethyl acetate in hexane to separate **3** (yield: 5 mg, 40%). For **4a**, ^{1}H NMR (400 MHz, acetonitrile-d_3) δ 7.36 (s, 2H), 7.11 (s, 4H), 2.37 (s, 6H), 2.11 (s, 12H); ^{13}C NMR (101 MHz, chloroform-*d*): δ 173.29, 139.73, 134.64, 134.59, 129.44, 122.13, 21.11, 17.73. For **3**, ^{1}H NMR (400 MHz, chloroform-d) δ 16.33 (s, 0H), 8.56 (d, J = 4.4 Hz, 1H), 8.00 (d, J = 7.8 Hz, 1H), 7.86 (t, J = 7.7, 1H), 7.55 (t, J = 7.6, 1H), 7.48 (t, J = 7.5, 1.4 Hz, 1H), 7.42 (dd, J = 7.6, 1.3 Hz, 1H), 7.28 (d, J = 1.5 Hz, 1H), 1.87 (s, 6H). ^{13}C NMR (101 MHz, chloroform-d) δ 197.71, 190.95, 154.88, 148.92, 140.69, 137.22, 135.69, 132.38, 131.17, 129.77, 127.73, 126.81, 123.45, 113.27, 24.40. LRMS (ES-API) (methanol, *m*/*z*): calcd for $C_{17}H_{16}NO_3$ [M + H] 282.1, found: 282.1.

Synthesis of Au(IDip)Cl (4b). Under normal atmospheric conditions, dichloro(2-benzoylpyridine)gold(III), **1** (22 mg, 0.049 mmol) and **2b** (22 mg, 0.053 mmol) were dissolved in 5 ml of 1,4-dioxane with NBu_4(acac) (33 mg, 0.096 mmol), and the solution was stirred and refluxed at 110 °C for 90 minutes. The color changed to purple and the reaction solution was monitored by TLC in 5% MeOH in DCM. **4b** showed a spot of $R_f \sim 0.9$ and $R_f \sim 0.8$ is for **3** on TLC. The product was separ-

ated by flash silica-gel chromatography with gradient elution (0 to 5% MeOH in DCM) (**4b**: yield: 15 mg, 56% and **3**: yield: 7 mg, 47%). For **4b**, ^{1}H NMR (400 MHz, chloroform-*d*) δ 7.48 (dd, J = 8.1, 7.5 Hz 1H), 7.27 (d, J = 7.8 Hz, 2H), 7.15 (s, 1H), 2.54 (hept, J = 6.8 Hz, 2H), 1.33 (d, J = 6.9 Hz, 6H), 1.20 (d, J = 6.9 Hz, 6H); ^{13}C NMR (101 MHz, chloroform-*d*) δ 175.42, 145.55, 133.94, 130.70, 124.23, 123.02, 77.30, 76.98, 76.66, 28.79, 24.43, 24.00; HRMS (ESI) (DCM, *m*/*z*): calcd for $C_{27}H_{36}AuClN_2$ [M + Na] 643.2130, found: 643.2137.

Synthesis of Au(IOH)Cl (4c). Under normal atmospheric conditions, dichloro(2-benzoylpyridine)gold(III), **1** (25 mg, 0.056 mmol) and **2c** (16 mg, 0.056 mmol) were dissolved in 6 ml of 1,4-dioxane with NBu_4(acac) (40 mg, 0.116 mmol), and the solution was stirred and refluxed at 110 °C for 40 min. The reaction was monitored by TLC in 5% MeOH in DCM and the solution color was purple at completion. **3** showed a spot of $R_f \sim 0.8$ and $R_f \sim 0.5$ is for **4c** on TLC. **4c** and **3** were separated by silica-gel chromatography with 25% ethyl acetate in hexane as the eluent (**4c**: yield: 4 mg, 14% and **3**: yield: 7 mg, 44%, respectively). For **4c**, ^{1}H NMR (400 MHz, DMSO-d_6) δ 9.97 (s, 2H), 7.88 (s, 2H), 7.55 (d, J = 8.7 Hz, 4H), 6.92 (d, J = 8.6 Hz, 4H). ^{13}C NMR (101 MHz, DMSO-d_6) δ 167.74, 157.97, 130.67, 126.51, 123.24, 115.79. Anal. Calc. for $C_{15}H_{12}AuClN_2O_2$ $0.87C_6H_{14}$: C 43.39; H 4.35; N 5.01. Found: C 43.99; H 3.77; N 5.18. For **3**, ^{1}H NMR (400 MHz, chloroform-d) δ 8.56 (d, J = 4.8 Hz, 1H), 8.00 (d, J = 7.8 Hz, 1H), 7.86 (t, J = 7.7 Hz, 1H), 7.61 (d, J = 7.5 Hz, 1H), 7.55 (t, J = 7.5 Hz, 1H), 7.48 (t, J = 7.6 Hz, 1H), 7.42 (dd, J = 7.6, 4.8 Hz, 1H), 7.27 (d, J = 7.4 Hz, 1H), 1.87 (s, 6H). ^{13}C NMR (101 MHz, chloroform-d) δ 197.73, 190.98, 154.82, 148.92, 140.63, 137.25, 135.66, 132.38, 131.20, 129.76, 127.75, 126.85, 123.46, 113.25, 24.43.

Au(ICy)BF$_4$ (4d). Under normal atmospheric conditions, dichloro(2-benzoylpyridine)gold(III), **1** (21 mg, 0.046 mmol) and **2d** (15 mg, 0.046 mmol) were dissolved in 5 ml of 1,4-dioxane with NBu_4(acac) (32 mg, 0.093 mmol), and the solution was stirred and refluxed at 110 °C for 15 minutes. The color changed from pale yellow to purple and the reaction solution was monitored by TLC in 5% MeOH in DCM. **4d** showed a spot of $R_f \sim 0.9$ and $R_f \sim 0.5$ is for **3** on TLC. **4d** was separated by silica-gel chromatography with DCM as the eluent (yield: 12 mg, 56%) and then the eluent was changed to 25% ethyl acetate in hexane to separate **3** (yield: 1 mg, ~7%). For **4d**, ^{1}H NMR (400 MHz, DMSO-d_6) δ 7.59 (s, 2H), 4.45–4.33 (m, 2H), 1.97–1.88 (m, 4H), 1.87–1.69 (m, 8H), 1.67 (d, J = 12.9 Hz, 2H), 1.39 (q, J = 13.2, 12.6 Hz, 4H), 1.26–1.11 (m, 2H); ^{13}C NMR (101 MHz, chloroform-*d*) δ 168.27, 117.12, 77.33, 77.01, 76.69, 60.90, 34.02, 25.27, 25.05; HRMS (ESI) (DCM, *m*/*z*): calcd for $C_{15}H_{24}AuClN_2$ [M + Na] 487.1191, found: 487.1187.

Synthesis of Au(I*t*Bu)BF$_4$ (4e). Under normal atmospheric conditions, dichloro(2-benzoylpyridine)gold(III), **1** (20 mg, 0.04 mmol) and **2e** (12 mg, 0.04 mmol) were dissolved in 5 ml of 1,4-dioxane with NBu_4(acac) (29 mg, 0.09 mmol), and the solution was stirred and refluxed at 110 °C for 10 minutes. The color changed to purple and the reaction solution was monitored by TLC in 50% ethyl acetate in hexane. **3** showed a spot of $R_f \sim 0.9$ and $R_f \sim 0.5$ is for **4e** on TLC. **4e** and **3** were separated by silica-gel chromatography with 50% ethyl acetate in hexane (for **4e**, yield: 16 mg, 88% and for **3**, yield: 9 mg, 73%). For **4e**, ^{1}H NMR (400 MHz, DMSO-d_6) δ 7.50 (s, 2H), 1.80 (s, 18H). ^{13}C NMR (101 MHz, DMSO-d_6) δ 165.81, 117.78, 58.44, 31.18; HRMS (ESI) (DCM, *m*/*z*): calcd for $C_{11}H_{20}AuClN_2$ [M + Na] 435.0878, found: 435.0875.

Synthesis of Au(IMes)Cl (4a) with 1′. Under normal atmospheric conditions, dichloro(2-benzylpyridine)gold(III), **1′** (20 mg, 0.04 mmol) and **2a** (15 mg, 0.04 mmol) were dissolved in 5 ml of 1,4-dioxane with NBu_4(acac) (30 mg, 0.09 mmol), and the solution was stirred and refluxed at 110 °C for 10 minutes. The color changed to pale purple and the reaction solution was monitored by TLC in 25% ethyl acetate in hexane. **3′** showed a spot of $R_f \sim 0.9$ and $R_f \sim 0.5$ is for **4a** on the TLC plate. **3′** and **4a** were separated by silica-gel chromatography with 25% ethyl acetate in hexane (for **4a**, yield: 12 mg, 51% and for **3′**, yield: 7 mg, 56%). For **3**, ^{1}H NMR (400 MHz, chloroform-d) δ 8.50 (d, J = 4.9 Hz, 1H), 7.56 (td, J = 7.6, 1.9 Hz, 1H), 7.39 (d, J = 7.9 Hz, 1H), 7.34 (td, J = 7.5, 1.6 Hz, 1H), 7.27 (td, J = 7.4, 1.6 Hz, 1H), 7.14–7.05 (m, 2H), 7.02 (d, J = 7.9 Hz, 1H), 4.02 (s, 2H), 1.63 (s, 6H). ^{13}C NMR (101 MHz, $CDCl_3$) δ 191.13, 160.14, 149.71, 139.72, 136.54, 136.42, 132.12, 131.17, 128.55, 127.50, 123.62, 121.40, 113.53, 77.48, 77.16, 76.84, 42.85, 23.83; LRMS (ESI) (methanol, *m*/*z*): calcd for $C_{17}H_{18}NO_2$ [M + H] 268.1338, found: 268.13.

Synthesis of Au(IDip)Cl (4b) with 1′. Under normal atmospheric conditions, dichloro(2-benzylpyridine)gold(III), **1′** (20 mg, 0.04 mmol) and **2b′** (19 mg, 0.04 mmol) were dissolved in 5 ml of 1,4-dioxane with NBu_4(acac) (30 mg, 0.09 mmol), and the solution was stirred and refluxed at 110 °C for 10 minutes. The color changed to pale purple and the reaction solution was monitored by TLC in 25% ethyl acetate in hexane. **3′** showed a spot of $R_f \sim 0.9$ and $R_f \sim 0.5$ is for **4b′** on the TLC plate. **4b′** and **3′** were separated by silica-gel chromatography with 25% ethyl acetate in hexane (for **4b′**, yield: 10 mg, 37% and for **3′**, yield: 6 mg, 48%).

Synthesis of Au(IOH)Cl (4c) with 1′. Under normal atmospheric conditions, dichloro(2-benzylpyridine)gold(III), **1′** (20 mg, 0.04 mmol) and **2c′** (13 mg, 0.04 mmol) were dissolved in 5 ml of 1,4-dioxane with NBu_4(acac) (30 mg, 0.09 mmol), and the solution was stirred and refluxed at 110 °C for 10 minutes. The color changed to pale purple and the reaction solution was monitored by TLC in 25% ethyl acetate in hexane. **3′** showed a spot of $R_f \sim 0.9$ and $R_f \sim 0.5$ is for **4c′** on the TLC plate. **4c′** and **3′** were separated by silica-gel chromatography with 25% ethyl acetate in hexane (for **4c′**, yield: 9 mg, 42% and for **3′**, yield: 9 mg, 73%).

Au(ICy)BF$_4$ (4d) with 1′. Under normal atmospheric conditions, dichloro(2-benzylpyridine)gold(III), **1′** (20 mg, 0.04 mmol) and **2d′** (15 mg, 0.05 mmol) were dissolved in 5 ml of 1,4-dioxane with NBu_4(acac) (30 mg, 0.09 mmol), and the solution was stirred and refluxed at 110 °C for 10 minutes. The color changed to pale purple and the reaction solution was monitored by TLC in 25% ethyl acetate in hexane. **3′** showed a spot of $R_f \sim 0.9$ and $R_f \sim 0.5$ is for **4d′** on the TLC plate. **4d′**

and **3′** were separated by silica-gel chromatography with 25% ethyl acetate in hexane (for **4d′**, yield: 8 mg, 39% and for **3′**, yield: 5 mg, 40%).

Synthesis of Au(I*t*Bu)BF_4 (4e) with 1′. Under normal atmospheric conditions, dichloro(2-benzylpyridine)gold(III), **1′** (20 mg, 0.04 mmol) and **2e′** (12 mg, 0.04 mmol) were dissolved in 5 ml of 1,4-dioxane with NBu_4(acac) (31 mg, 0.09 mmol), and the solution was stirred and refluxed at 110 °C for 10 minutes. The color changed to pale purple and the reaction solution was monitored by TLC in 25% ethyl acetate in hexane. **3′** showed a spot of $R_f \sim 0.9$ and $R_f \sim 0.5$ is for **4e′** on the TLC plate. **4e′** and **3′** were separated by silica-gel chromatography with 25% ethyl acetate in hexane (for **4e′**, yield: 11 mg, 60% and for **3′**, yield: 8 mg, 64%).

Reaction of 1 + 2f. Under normal atmospheric conditions, dichloro(2-benzoylpyridine)gold(III), **1** (20 mg, 0.04 mmol) and (*R*,*R*)-(−)-2,3-bis(*t*-butylmethylphosphino)quinoxaline, **2f** (15 mg, 0.04 mmol), were dissolved in 5 ml of dichloromethane. The reaction solution was stirred at room temperature. The color changed to purple and the reaction solution was monitored by TLC in 5% methanol in dichloromethane. The R_f of **3** is ∼0.0 and the R_f of bis-[2,3-bis(*tert*-butylmethylphosphino)quinoxaline]gold(I) chloride is ∼0.3 on TLC. Bis-[2,3-bis(*tert*-butylmethylphosphino)quinoxaline]gold(I) chloride was separated by silica-gel chromatography with 5% methanol in DCM and **3** was isolated by putting **3**-absorbed-silica(dark gray) in CH_3CN with sonication after using 100% MeOH as the eluent (for **3**, yield: 12 mg, 57% and for bis-[2,3-bis(*tert*-butylmethylphosphino)quinoxaline] gold(I) chloride, yield: 22 mg, 25%). LRMS (ESI) (MeOH, *m*/*z*): calcd for **3**, $C_{12}H_8NO^+$ [MH + H] 184.1, found: 184.1.

Kinetic modeling of reductive elimination from the reaction

(*C*,*N*)-Cyclometalated Au(III) (1) + IMes·Cl (2a). Under normal atmospheric conditions, dichloro(2-benzoylpyridine)gold(III), **1** (30.0 mg, 0.07 mmol) and IMes·Cl, **2a** (23 mg, 0.07 mmol), were dissolved in 7 ml of CD_3CN. The reaction mixture was separated into 7 vials, to which different amounts of NBu_4(acac) (0, 0.75, 1.00, 1.25, 1.50, 1.75, and 2 equiv.) were added. After thorough mixing, the reaction solution was transferred to NMR tubes, and quickly inserted into the preheated (80 °C) NMR probe and ^{1}H NMR spectra were collected at 60 s intervals. Twenty spectra were obtained for each NMR tube. During each scan, the NMR tubes were spun at 20 Hz. In order to investigate the reactant and product change, two NMR peaks were chosen: 7.17 ppm for the reactant and 7.12 ppm for the product. The former corresponds to the proton of the benzene ring of free **2a**, and the latter to the proton of the benzene ring in Au(IMes)Cl, **4a**.

(*C*,*N*)-Cyclometalated Au(III) (1) + I*t*Bu-BF_4 (2e). Under normal atmospheric conditions, dichloro(2-benzoylpyridine) gold(III), **1** (30.0 mg, 0.07 mmol) and I*t*Bu·BF_4, **2e** (18 mg, 0.07 mmol), were dissolved in 7 ml of CD_3CN. The reaction mixture was separated into 7 vials, to which different amounts of NBu_4(acac) (0, 0.75, 1.00, 1.25, 1.50, 1.75, and 2 equiv.) were added. After thorough mixing, the reaction solution was transferred to NMR tubes, and quickly inserted into the preheated (80 °C) NMR probe and ^{1}H NMR spectra were collected at 60 s intervals. Twenty spectra were obtained for each NMR tube. During each scan, NMR tubes were spun at 20 Hz. In order to investigate the reactant and product changes, two NMR peaks were chosen: 7.60 ppm for the reactant and 7.28 ppm for the product. The former corresponds to the proton of the imidazole ring of free **2e**, and the latter to the proton of the imidazole ring in Au(I*t*Bu)BF_4, **4e**.

(*C*,*N*)-Cyclometalated Au(III) (1′) + IMes·Cl (2a). Under normal atmospheric conditions, dichloro(2-benzylpyridine) gold(III), **1′** (4 mg, 0.01 mmol) and IMes·Cl, **2a** (4 mg, 0.01 mmol), were dissolved in 1 ml of CD_3CN. 1.75 equiv. of NBu_4(acac) was added. After thorough mixing, the reaction solution was transferred to NMR tubes, and quickly inserted into the preheated (80 °C) NMR probe and ^{1}H NMR spectra were collected at 60 s intervals. Twenty spectra were obtained. During each scan, NMR tubes were spun at 20 Hz. In order to investigate the reactant and product changes, two NMR peaks were chosen: 7.17 ppm for the reactant and 7.12 ppm for the product. The former corresponds to the proton of the benzene ring of free **2a**, and the latter to the proton of the benzene ring in Au(IMes)Cl, **4a′**.

Computational details

Calculations were performed using Gaussian16 Rev. A.03. Geometries of the investigated systems were fully optimized at the spin-restricted density functional theory level using the dispersion-corrected ωB97x-D exchange–correlation functional.[46] The balanced polarized triple-zeta quality basis set def2-TZVP from Ahlrichs and co-workers[47,48] has been used for all atoms, and it comprises the use of a quasi-relativistic Stuttgart-Dresden core potential for the Au metal center. For the calculation of Fukui indices, an all-electron scalar relativistic approximation (zeroth order regular approximation, ZORA)[41] was used as implemented in ORCA 4.[42] Potential energy surface minima found upon optimization were confirmed by frequency calculations and free energies were corrected to account for the zero-point energy. Optimized geometries were verified as minima (*i.e.* zero imaginary frequencies). The Synchronous Transit-Guided Quasi-Newton (STQN) method[49,50] was used for locating the transition structures and these were verified as first-order saddle points by frequency calculations (*i.e.* one and only one imaginary frequency). Transition structures were further verified to connect the desired reactants and products by integrating the intrinsic reaction coordinate,[51] using the Hessian-based predictor–corrector integrator.[52] These reaction paths were calculated using the split valence version of the basis set (def2-SVP), recomputing the analytical Hessian at each point. The bulk solvent effects were included through the Integral Equation Formalism version of the Polarizable Continuum Model (IEF-PCM).[53] Oxidation states of key intermediates were determined using localized orbital bonding analysis (LOBA) as implemented in the Q-Chem code (QChem 5.0).[54]

Conclusion

In summary, we uncovered the first direct, intramolecular C(sp^2)–N(sp^2) bond formation from rigid (*C*,*N*)-cyclometalated gold backbones proceeding *via* second-order kinetics. Using rigid cyclometalated gold(III), we systematically studied its C(sp^2)–N(sp^2) bond reductive elimination process and applied DFT calculations to elucidate the potential mechanism. We discovered key Au(III) intermediates (**IM1** and **IM2**), which support an associative ligand pathway. The mechanism and scope of these reactions broaden our understanding of ligand-induced reductive elimination reactions using Au(III) and provide strategies to achieve C–N bond formation and obtain Au(I) reagents for biological and electronic applications in a facile manner and at ambient temperature. This work ignites studies on underdeveloped gold-catalyzed C–N bond formation.

Conflicts of interest

There are no conflicts to declare.

Acknowledgements

We are grateful to the staff and facilities at the University of Kentucky that supported this work. This study made use of the NMR facility supported by NSF (CHE-9977388) and the UK X-ray facility with funds from the MRI program of the National Science Foundation (grants CHE-0319176 and CHE-1625732). Thanks to the staff of CIC, Boston University for running mass spectrometry samples. We thank Prof. Dong-Sheng Yang and Prof. John P. Selegue for helpful comments on kinetics and chemistry, respectively. G. B. thanks the ULB-VUB computing centre for providing high performance computing facilities and useful technical support.

Notes and references

1 A. S. Hashmi and G. J. Hutchings, Gold catalysis, *Angew. Chem., Int. Ed.*, 2006, **45**(47), 7896–7936.
2 R. H. Crabtree, in *The Organometallic Chemistry of the Transition Metals*, Wiley, Hoboken, NJ, 4th edn, 2005.
3 K. Tatsumi, A. Nakamura, S. Komiya, A. Yamamoto and T. Yamamoto, An associative mechanism for reductive elimination of d8 NiR2(PR3)2, *J. Am. Chem. Soc.*, 1984, **106**(26), 8181–8188.
4 K. Tatsumi, R. Hoffmann, A. Yamamoto and J. K. Stille, Reductive Elimination of d8-Organotransition Metal Complexes, *Bull. Chem. Soc. Jpn.*, 1981, **54**(6), 1857–1867.
5 M. S. Winston, W. J. Wolf and F. D. Toste, Halide-Dependent Mechanisms of Reductive Elimination from Gold(III), *J. Am. Chem. Soc.*, 2015, **137**(24), 7921–7928.
6 A. Moravskiy and J. K. Stille, Mechanisms of 1,1-reductive elimination from palladium: elimination of ethane from dimethylpalladium(II) and trimethylpalladium(IV), *J. Am. Chem. Soc.*, 1981, **103**(14), 4182–4186.
7 J. F. Hartwig, Carbon–Heteroatom Bond-Forming Reductive Eliminations of Amines, Ethers, and Sulfides, *Acc. Chem. Res.*, 1998, **31**(12), 852–860.
8 J. P. Wolfe, S. Wagaw, J.-F. Marcoux and S. L. Buchwald, Rational Development of Practical Catalysts for Aromatic Carbon–Nitrogen Bond Formation, *Acc. Chem. Res.*, 1998, **31**(12), 805–818.
9 C. M. Frech and D. Milstein, Direct Observation of Reductive Elimination of Methyl Iodide from a Rhodium (III) Pincer Complex: The Importance of Sterics, *J. Am. Chem. Soc.*, 2006, **128**(38), 12434–12435.
10 K. I. Goldberg, J. Y. Yan and E. L. Winter, Competitive Carbon-Carbon Reductive Elimination and Carbon-Iodide Bond Formation from a Pt(IV) Complex, *J. Am. Chem. Soc.*, 1994, **116**(4), 1573–1574.
11 B. S. Williams, A. W. Holland and K. I. Goldberg, Direct Observation of C–O Reductive Elimination from Pt(IV), *J. Am. Chem. Soc.*, 1999, **121**(1), 252–253.
12 T. E. Stevens, K. A. Smoll and K. I. Goldberg, Direct Formation of Carbon(sp3)–Heteroatom Bonds from RhIII To Produce Methyl Iodide, Thioethers, and Alkylamines, *J. Am. Chem. Soc.*, 2017, **139**(23), 7725–7728.
13 T. Furuya, D. Benitez, E. Tkatchouk, A. E. Strom, P. Tang, W. A. Goddard and T. Ritter, Mechanism of C–F Reductive Elimination from Palladium(IV) Fluorides, *J. Am. Chem. Soc.*, 2010, **132**(11), 3793–3807.
14 N. M. Camasso and M. S. Sanford, Design, synthesis, and carbon-heteroatom coupling reactions of organometallic nickel(IV) complexes, *Science*, 2015, **347**(6227), 1218–1220.
15 A. S. Hashmi, Catalysis: raising the gold standard, *Nature*, 2007, **449**(7160), 292–293.
16 A. S. Hashmi, Gold-catalyzed organic reactions, *Chem. Rev.*, 2007, **107**(7), 3180–3211.
17 D. J. Gorin, B. D. Sherry and F. D. Toste, Ligand effects in homogeneous Au catalysis, *Chem. Rev.*, 2008, **108**(8), 3351–3378.
18 K. I. Goldberg, J. Yan and E. M. Breitung, Energetics and Mechanisms of Carbon-Carbon and Carbon-Iodide Reductive Elimination from a Pt(IV) Center, *J. Am. Chem. Soc.*, 1995, **117**(26), 6889–6896.
19 A. H. Roy and J. F. Hartwig, Directly Observed Reductive Elimination of Aryl Halides from Monomeric Arylpalladium(II) Halide Complexes, *J. Am. Chem. Soc.*, 2003, **125**(46), 13944–13945.
20 S. Komiya and J. K. Kochi, Electrophilic cleavage of organogold complexes with acids. The mechanism of the reductive elimination of dialkyl(aniono)gold(III)species, *J. Am. Chem. Soc.*, 1976, **98**, 7599–7607.
21 S. Komiya, T. A. Albright, R. Hoffmann and J. K. Kochi, Reductive elimination and isomerization of organogold complexes. Theoretical studies of trialkylgold species as reactive intermediates, *J. Am. Chem. Soc.*, 1976, **98**, 7255–7265.
22 A. Tamaki, S. A. Magennis and J. K. Kochi, Catalysis by gold. Alkyl isomerization, *cis-trans* rearrangement, and

reductive elimination of alkygold(III) complexes, *J. Am. Chem. Soc.*, 1974, **96**, 6140–6148.

23 P. L. Kuch and R. S. Tobias, Synthesis of cationic dialkylgold(III) complexes: nature of the facile reductive elimination of alkane, *J. Organomet. Chem.*, 1976, **122**, 429–446.

24 J. Vicente, M. Dolores Bermudez and J. Escribano, Gold in organic synthesis. Preparation of symmetrical and unsymmetrical biaryls via carbon-carbon coupling from cis-diarylgold(III) complexes, *Organometallics*, 1991, **10**(9), 3380–3384.

25 J. Vicente, M. D. Bermudez, J. Escribano, M. P. Carrillo and P. G. Jones, Synthesis of intermediates in the C–H activation of acetone with 2-phenylazophenylgold(III) complexes and in the C–C coupling of aryl groups from diarylgold(III) complexes. Crystal and molecular structures of [Au{C6H3(N=NC6H4Me-4′)-2-Me-5}(acac-C)Cl](acac =acetylacetonate), cis-[Au(C6H4N=NPh-2)Cl2(PPh3)] and [Au(C6H4CH2NMe2-2)(C6F5)Cl], *J. Chem. Soc., Dalton Trans.*, 1990, 3083–3089.

26 W. J. Wolf, M. S. Winston and F. D. Toste, Exceptionally fast carbon-carbon bond reductive elimination from gold (III), *Nat. Chem.*, 2014, **6**(2), 159–164.

27 N. P. Mankad and F. D. Toste, C(sp(3))-F reductive elimination from alkylgold(III) fluoride complexes, *Chem. Sci.*, 2012, **3**(1), 72–76.

28 R. Kumar, A. Linden and C. Nevado, Evidence for Direct Transmetalation of AuIII–F with Boronic Acids, *J. Am. Chem. Soc.*, 2016, **138**(42), 13790–13793.

29 K. Kang, S. Liu, T. Xu, D. Wang, X. Leng, R. Bai, Y. Lan and Q. Shen, C(sp2)–C(sp2) Reductive Elimination from Well-Defined Diarylgold(III) Complexes, *Organometallics*, 2017, **36**(24), 4727–4740.

30 T. J. A. Corrie, L. T. Ball, C. A. Russell and G. C. Lloyd-Jones, Au-Catalyzed Biaryl Coupling To Generate 5- to 9-Membered Rings: Turnover-Limiting Reductive Elimination versus π-Complexation, *J. Am. Chem. Soc.*, 2017, **139**(1), 245–254.

31 M. J. Harper, C. J. Arthur, J. Crosby, E. J. Emmett, R. L. Falconer, A. J. Fensham-Smith, P. J. Gates, T. Leman, J. E. McGrady, J. F. Bower and C. A. Russell, Oxidative Addition, Transmetalation, and Reductive Elimination at a 2,2′-Bipyridyl-Ligated Gold Center, *J. Am. Chem. Soc.*, 2018, **140**(12), 4440–4445.

32 J. Serra, C. J. Whiteoak, F. Acuña-Parés, M. Font, J. M. Luis, J. Lloret-Fillol and X. Ribas, Oxidant-Free Au(I)-Catalyzed Halide Exchange and Csp2–O Bond Forming Reactions, *J. Am. Chem. Soc.*, 2015, **137**(41), 13389–13397.

33 H. Kawai, W. J. Wolf, A. G. DiPasquale, M. S. Winston and F. D. Toste, Phosphonium Formation by Facile Carbon–Phosphorus Reductive Elimination from Gold(III), *J. Am. Chem. Soc.*, 2016, **138**(2), 587–593.

34 J. Serra, T. Parella and X. Ribas, Au(III)-aryl intermediates in oxidant-free C-N and C-O cross-coupling catalysis, *Chem. Sci.*, 2017, **8**(2), 946–952.

35 S. Lavy, J. J. Miller, M. Pažický, A.-S. Rodrigues, F. Rominger, C. Jäkel, D. Serra, N. Vinokurov and M. Limbach, Stoichiometric Reductive C–N Bond Formation of Arylgold(III) Complexes with N-Nucleophiles, *Adv. Synth. Catal.*, 2010, **352**(17), 2993–3000.

36 M. Joost, A. Amgoune and D. Bourissou, Reactivity of Gold Complexes towards Elementary Organometallic Reactions, *Angew. Chem., Int. Ed.*, 2015, **54**(50), 15022–15045.

37 Y. Fuchita, H. Ieda, Y. Tsunemune, J. Kinoshita-Nagaoka and H. Kawano, Synthesis, structure and reactivity of a new six-membered cycloaurated complex of 2-benzoylpyridine [AuCl2(pcp-C 1,N)] [pcp[space]=[space]2-(2-pyridylcarbonyl) phenyl]. Comparison with the cycloaurated complex derived from 2-benzylpyridine, *J. Chem. Soc., Dalton Trans.*, 1998, (5), 791–796.

38 M. A. S. Goher, A. E. H. Abdou, B.-S. Luo and T. C. W. Mak, Intramolecular oxidative cyclization of 2-benzoylpyridine and structural characterization of [9-oxo-indolo[1,2-a]pyridinium] copperdiiodide and [di-μ-bromo-bis(2-benzoylpyridine)dicopper(I)], *J. Coord. Chem.*, 1995, **36**(1), 71–80.

39 A. Levens, F. An, M. Breugst, H. Mayr and D. W. Lupton, Influence of the N-Substituents on the Nucleophilicity and Lewis Basicity of N-Heterocyclic Carbenes, *Org. Lett.*, 2016, **18**(15), 3566–3569.

40 G. Berger, Using conceptual density functional theory to rationalize regioselectivity: A case study on the nucleophilic ring-opening of activated aziridines, *Comput. Theor. Chem.*, 2013, **1010**, 11–18.

41 E. v. Lenthe, E. J. Baerends and J. G. Snijders, Relativistic regular two-component Hamiltonians, *J. Chem. Phys.*, 1993, **99**(6), 4597–4610.

42 F. Neese, The ORCA program system, *Wiley Interdiscip. Rev.: Comput. Mol. Sci.*, 2012, **2**(1), 73–78.

43 H. von Wachenfeldt, A. V. Polukeev, N. Loganathan, F. Paulsen, P. Röse, M. Garreau, O. F. Wendt and D. Strand, Cyclometallated gold(iii) aryl-pyridine complexes as efficient catalysts for three-component synthesis of substituted oxazoles, *Dalton Trans.*, 2015, **44**(12), 5347–5353.

44 K. K.-Y. Kung, V. K.-Y. Lo, H.-M. Ko, G.-L. Li, P.-Y. Chan, K.-C. Leung, Z. Zhou, M.-Z. Wang, C.-M. Che and M.-K. Wong, Cyclometallated gold(III) complexes as effective catalysts for synthesis of propargylic amines, chiral allenes and isoxazoles, *Adv. Synth. Catal.*, 2013, **355**(10), 2055–2070.

45 M. J. Frisch, G. W. Trucks, H. B. Schlegel, G. E. Scuseria, M. A. Robb, J. R. Cheeseman, G. Scalmani, V. Barone, G. A. Petersson, H. Nakatsuji, X. Li, M. Caricato, A. V. Marenich, J. Bloino, B. G. Janesko, R. Gomperts, B. Mennucci, H. P. Hratchian, J. V. Ortiz, A. F. Izmaylov, J. L. Sonnenberg, D. Williams-Young, F. Ding, F. Lipparini, F. Egidi, J. Goings, B. Peng, A. Petrone, T. Henderson, D. Ranasinghe, V. G. Zakrzewski, J. Gao, N. Rega, G. Zheng, W. Liang, M. Hada, M. Ehara, K. Toyota, R. Fukuda, J. Hasegawa, M. Ishida, T. Nakajima, Y. Honda, O. Kitao, H. Nakai, T. Vreven, K. Throssell, J. A. Montgomery Jr., J. E. Peralta, F. Ogliaro, M. J. Bearpark, J. J. Heyd, E. N. Brothers, K. N. Kudin, V. N. Staroverov, T. A. Keith, R. Kobayashi, J. Normand, K. Raghavachari, A. P. Rendell, J. C. Burant, S. S. Iyengar, J. Tomasi, M. Cossi,

J. M. Millam, M. Klene, C. Adamo, R. Cammi, J. W. Ochterski, R. L. Martin, K. Morokuma, O. Farkas, J. B. Foresman and D. J. Fox, *Gaussian 09, Revision E.01*, Wallingford, CT, 2016.

46 J. D. Chai and M. Head-Gordon, Long-range corrected hybrid density functionals with damped atom-atom dispersion corrections, *Phys. Chem. Chem. Phys.*, 2008, **10**(44), 6615–6620.

47 F. Weigend and R. Ahlrichs, Balanced basis sets of split valence, triple zeta valence and quadruple zeta valence quality for H to Rn: Design and assessment of accuracy, *Phys. Chem. Chem. Phys.*, 2005, **7**(18), 3297–3305.

48 F. Weigend, Accurate Coulomb-fitting basis sets for H to Rn, *Phys. Chem. Chem. Phys.*, 2006, **8**(9), 1057–1065.

49 C. Peng and H. B. Schlegel, Combining Synchronous Transit and Quasi-Newton Methods to Find Transition States, *Isr. J. Chem.*, 1993, **33**(4), 449–454.

50 C. Peng, P. Y. Ayala, H. B. Schlegel and M. J. Frisch, Using redundant internal coordinates to optimize equilibrium geometries and transition states, *J. Comput. Chem.*, 1996, **17**(1), 49–56.

51 K. Fukui, The path of chemical reactions - the IRC approach, *Acc. Chem. Res.*, 1981, **14**(12), 363–368.

52 H. P. Hratchian and H. B. Schlegel, *Theory and Applications of Computational Chemistry: The First 40 Years*, Elsevier, Amsterdam, 2005.

53 J. Tomasi, B. Mennucci and R. Cammi, Quantum mechanical continuum solvation models, *Chem. Rev.*, 2005, **105**(8), 2999–3093.

54 A. J. Thom, E. J. Sundstrom and M. Head-Gordon, LOBA: a localized orbital bonding analysis to calculate oxidation states, with application to a model water oxidation catalyst, *Phys. Chem. Chem. Phys.*, 2009, **11**(47), 11297–11304.

